OROGRAPHICALLY-GENERATED MESOSCALE PRECIPITATION SYSTEM IN NORTHERN TAIWAN: SINGLE DOPPLER RADAR ANALYSIS

BEN JONG-DAO JOU and YUH-SHII CHIN

Department of Atmospheric Sciences
National Taiwan University
Taipei, Taiwan, ROC

1. Introduction

Storm movement and propagation can be classified into three different mechanisms: (i) translation or advection, (ii) forced propagation, and (iii) autopropagation (Cotton and Anthes, 1989). Translation or advection is the process whereby a storm is blown along by the mean wind as it evolves through its lifetime. Forced propagation refers to the sustained regeneration of a convective storm by some external forcing mechanism usually larger in scale than the convective storm. Examples include fronts, rainband convergence in midlatitude cyclones, sea-breeze fronts, and convergence associated with mountains. Often the systems providing the forced propagation have lifetimes much longer than individual thunderstorms. Autopropagation refers to the process in which a thunderstorm can regenerate itself or cause the generation of similar storm cells within the same general system. Examples include downdraft forcing and gust fronts, and development of vertical pressure gradients due to storm rotation. Most convective systems are affected by all three mechanisms of movement and propagation for at least some part of their lifetime. In this study, we present a case in which an orographically-generated mesoscale convective precipitation system in northern Taiwan is described. The movement and propagation of the storm system is studied by using single Doppler radar located at CKS International airport in northern Taiwan. The interactions among the horizontal wind shear, the sea-breeze front, the mountain slope, and the storm-generated outflows are emphasized.

2. Data

Data used in this study were provided from a C-band Doppler radar at CKS International airport of the Civil Aeronautic Administration of Taiwan (CAA Doppler radar). The location of the radar is shown in Fig.1. Plan-position indicator (PPI) reflectivity and radial wind data, in time interval of 30 minutes, were gathered. Hourly satellite IR imagery and surface weather data from Central Weather Bureau were also used.

3. Case description

In 1991, a pilot program of TAMEX Forecast Experiment was held during May and June. One of the objectives of this program was to exercise the forecast skill on the torrential rain producer-mesoscale precipitation system (MPS) associated with the Mei-Yu front or generated by local circulation and rugged terrain derived from the scientific results of TAMEX field program held in 1987. It was a rather boring Mei-Yu season in the first one and half months during the Exercise. No significant events were encountered. However, at the end of June, the situation changed and became quite interesting. On the afternoon of 21 June 1991, a mountain-generated mesoscale precipitation system developed in the northern Taiwan. The storm system organized into a northeast-southwest line feature along the western mountain slope. More than 120 mm rain poured down to Taipei and Keelong (a harbor on the northern tip of Taiwan) within 3 hours. The maximum intensity on the record was 40 mm rain within 10 minutes (Keelong station). A severe flood was encounted over Taipei basin and Keelong city on that afternoon. The case caught our attention not only because it caused a severe flash flood problem in the most populated metropolitan area in Taiwan, but the roles of mountain on organization and propagation of the mesoscale precipitation systems is still a largely unresolved problem on mesoscale research in Taiwan.

a. Precipitation pattern

Fig.1 showed the hourly rainfall distribution over northern Taiwan during the period of interest. It showed there were two major precipitation centers, one at Keelong area and the other at Taipei basin. The rain at Keelong started at 1 pm on 21 June 1991 with trace amount and peaked to 28.5 mm at end of the hour (2 pm). In the next hour (3 pm), the accumulated rainfall hit the record high with rainfall intensity of 95.0 mm h^{-1}. The total accumulated rain between 1-4 pm at Keelong was 134.4 mm. The rain at Taipei basin started at 2 pm, an hour late than Keelong city. Within 3 hours (2-5 pm), the total accumulated rainfall was 140 mm with maximum rainfall rate of 94.5 mm h^{-1} at 4 pm. The rainfall data in this case showed the life period of the precipitation system was relatively short than the frontal precipitation system usually occurred in this season but lasted much longer than individual thunderstorm. It is also noted the heavy rain associated with the precipitation system was rather concentrated in terms of spatial and temporal scales. This precipitation character made the storm produce dangerous flash flood event in some local areas.

b. Synoptic conditions

Fig.2a showed the surface weather map at 0000 UTC (8 am) 21 June 1991. The surface front located north of Taiwan and approached to the Island very slowly. Deep but weak southwest monsoonal flow (up to 400 hPa) with warm and very moist air prevailed in northern Taiwan (see Fig.2b). The morning sounding of Panchiao (46692) showed that using parcel method the level of free convection was very low (988 hPa) and the atmosphere was convectively unstable with large CAPE (1818 $m^2 s^{-2}$). The surface temperature was 26.4°C in the morning and reached 33.1°C at 11:42 am (according to Taipei surface station observation). This data suggested on the morning of 21 June, there were plenty solar heating. Establishment of sea breeze over coastal area was anticipated, and thermally-driven afternoon thunderstorm shower type weather was forecasted. It is worth noting that the lower tropospheric winds were rather weak in the morning sounding (most of them were less than 10 knots below 900 hPa). No pre-frontal low-level jet existed on that day.

c. Evolution of the reflectivity pattern

Fig.3 showed the sequence of PPI (Plan-position indicator) radar reflectivity maps at elevation angle 4 from CAA C-band Doppler radar. In the figure, the first range mark is 60 km away from the radar, i.e., the radar target area at this distance is 4 km above the ground.

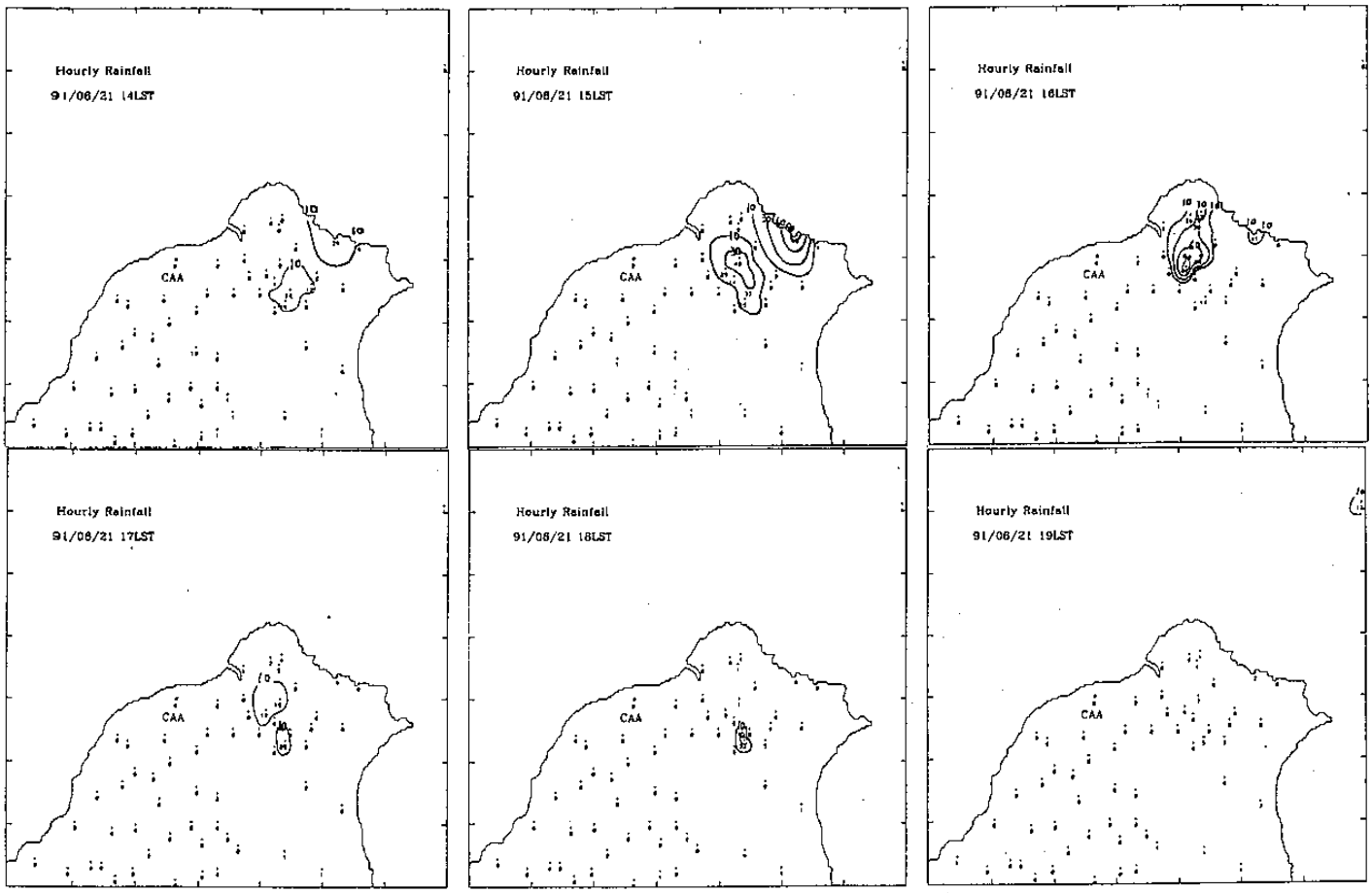

Fig.1. Surface rainfall rates distribution (in mm h^{-1}) in northern Taiwan from 2 pm (a) to 7 pm (f) on 21 June 1991. The contour is irregular (10, 30, 60 and 90 mm h^{-1}).

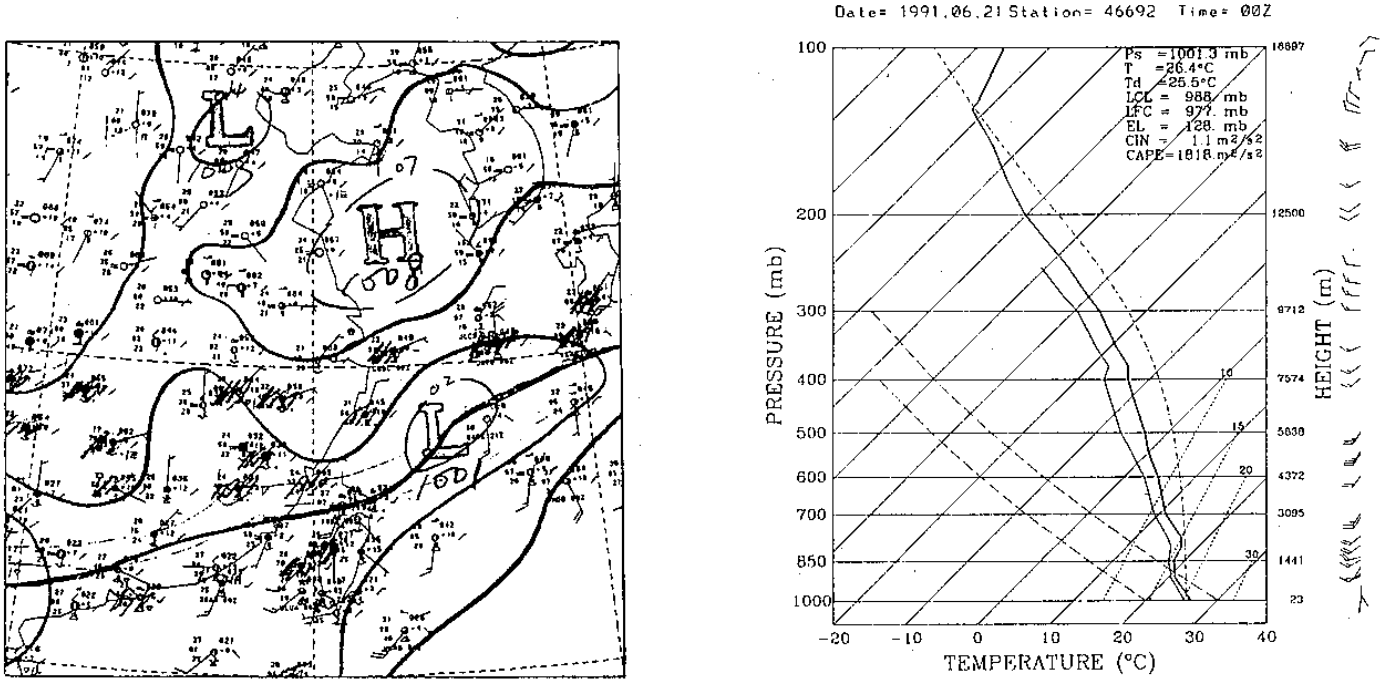

Fig.2. (a) Surface weather map for 0000 UTC 21 June 1991. (b) The skew T - log P presentation of sounding from Panchiao (46692) at 0000 UTC 21 June 1991. The short dash line represents the moist-adiabatic curve a hypothetically ascending surface parcel would have.

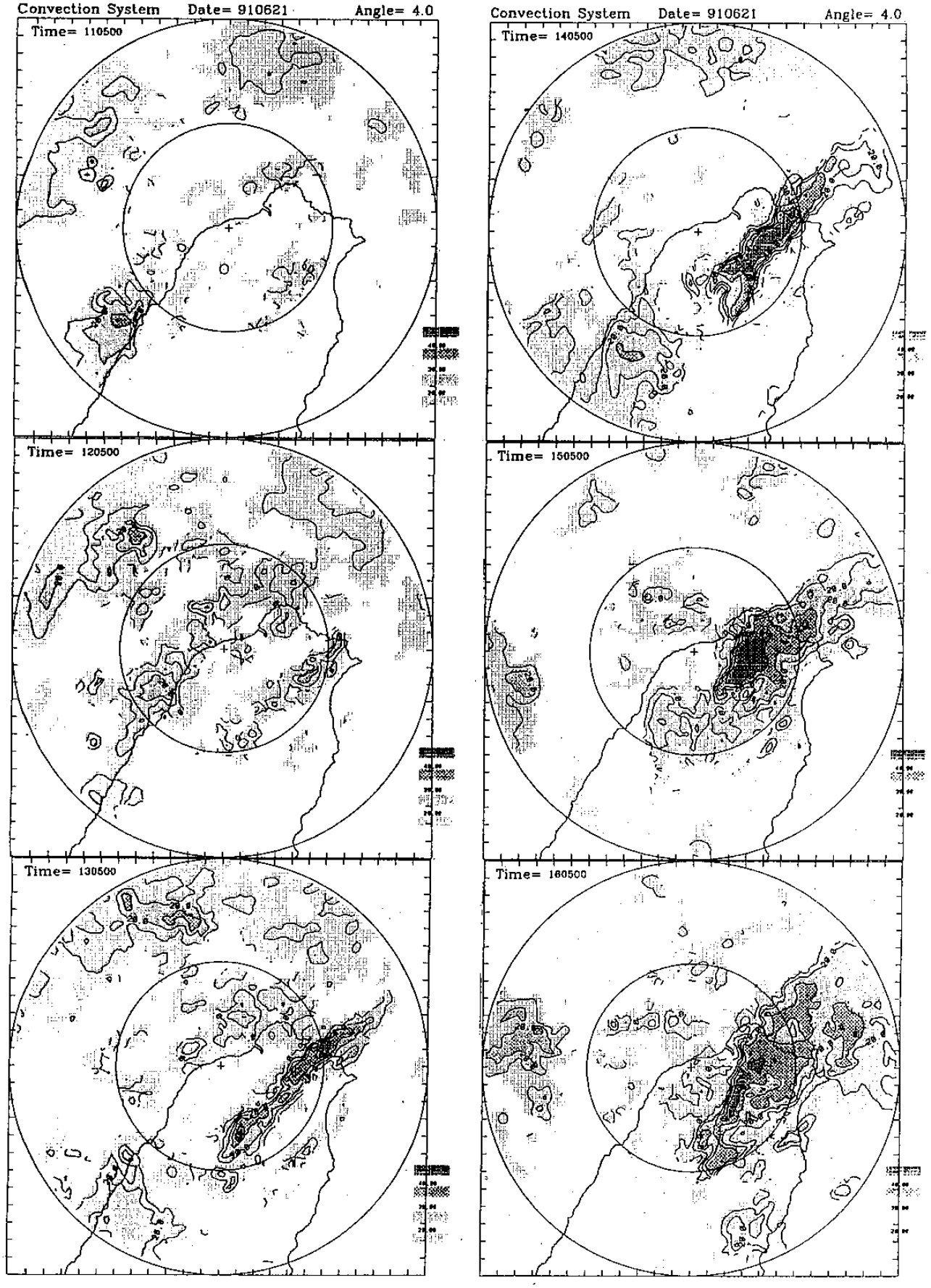

Fig.3. PPI scan radar reflectivity from CAA radar from 1105 (a) to 1605 LST (f) 21 June 1991. Beam elevation angle is 4.0 degree. The range marks are 60 and 120 km from the radar, respectively. The beginning contour is 10 dBZ. The contour interval is 10 dBZ.

The first echo was observed over the mountainous area southeast of Taipei basin. The early development of the echos were in a southwest-northeast orientation along the mountain ridge and gradually evolved into a line structure. At early stage, three major convective precipitation centers embedded within the line could be identified (see Fig.3c, 1305 LST). The storm intensity as represented by the radar reflectivity showed an explosive development as the system moved westward down the mountain slope. The major precipitation area (Z > 40 dBZ corresponding to a rainfall rate approximately 15 mm h^{-1}) became an elongated feature at 1405 LST (Fig.3d). This feature suggested storm merging process was quite efficient at this stage (Tao and Simpson, 1984). The storm reached its mature stage at around 1505 LST and decayed afterword (Figs.3e and 3f). It is noted the heavy precipitation area of the system at its mature stage occupied an area very similar to the geographic boundary of Taipei basin.

4. Storm movement and propagation

Fig.4 showed the 3 km constant-altitude plan position indicator (CAPPI) reflectivity map (1335 LST 21 June 1991) superimposed on terrain contours in northern Taiwan. In this figure, three major precipitation centers over land were vividly revealed. At this time, these storm centers were aligned into a line feature and propagated westward down the terrain slope. (Note: The geographic map had been rotated 45 counterclockwise, hence, the top of the map points toward northeastward.)

We traced the individual storm's trajectory by using sequential CAPPI reflectivity maps with 30 minute time interval. The results were shown in Fig.5. It can be seen each individual precipitation centers presented quite different trajectories. On the south of Taipei, the storm moved northeastward to the lower land. On the east of Taipei, the other two storms moved westward to the basin. The northeastward-propagating storm had a speed of 6.3 m/s. The westward-propagating storm A (toward the Keelong city) had a speed of 3.4 m/s, and storm B had a speed of 2.3 m/s in the sloping area and the movement became very slow in Taipei basin. It is also noted that the storm B moved northwestward in the sloping area and moved southwestward in the Taipei basin. This direction change occurred over the smaller mountain ridge at southeast of Taipei basin indicating a subtle relationship between the storm movement and the terrain features surrounding the city.

The propagation of each individual storm was investigated by time evolution of the maximum radar reflectivity in the vertical projected along a selected cross section. Fig.6a showed the cross section passing Taipei basin and Keelong city in northeast-southwest direction. The mean terrain feature was given at bottom of the figure. It can be seen the storm was initiated over the mountainous area and propagated northeastward down the mountain slope. At 1405 LST, the storm arrived southern tip of Taipei basin. At this time, the westward-propagating storm B also arrived Taipei basin from east. The result suggested storm merging process might play an important role in producing large area heavy precipitation in this case.

Fig.6b showed the time evolution maximum radar reflectivity cross section passing Taipei basin but in northwest-southeast direction. It is clear the storm was initiated over top of the mountain. At early developing stage, the storm did not propagate much and only possessed weak echos. The storm started to move downslope when echo intensity reached above 30 dBZ. Before moving into the basin, the storm stopped over the small ridge for a while and intensified significantly. The storm reached its mature stage at about 1505 LST and maintained its strength till 1535 LST and then decayed rapidly. According to Taipei surface station rainfall report, the storm brought 100 mm rain within an hour at the period, i.e., 1453-1553 LST, and had its 10 minute maximum rainfall rate (23 mm/10 minute) at 1515-1525 LST. Surface temperature dropped from 33.1 C at 1142 LST to 25.5 C at 1519 LST. Surface pressure increased from 999.8 hPa at 1357 LST to 1001.8 hPa at 1514 LST. Surface wind had changed abruptly from westerly to easterly at around 1500 LST. All these observations indicated a strong cold pool air associated with the heavy precipitation center propagated across the station at around 1515 LST. This cold pool air had a character of high pressure, low temperature, and sudden change of winds. Fig.6b also showed there was a second wave of convection initiated at sloping area at about 1600 LST. The convection propagated westward to the basin at about the same speed as the main system but with a much weaker intensity.

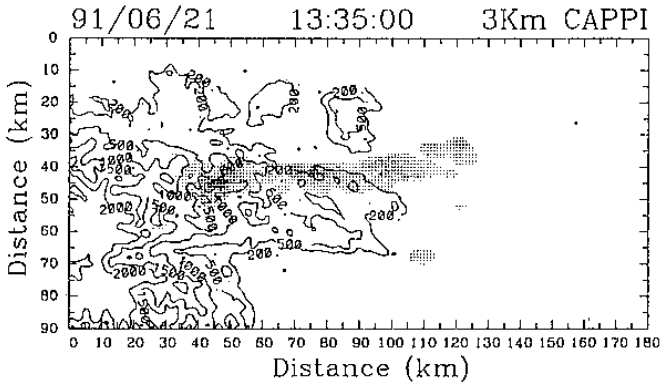

Fig.4. Radar reflectivity map at 3 km height derived from CAA radar on 1335 LST 21 June 1991. The beginning shading is 30 dBZ. The dark shading represents radar echo larger then 45 dBZ. The thin lines indicate the terrain contours (200m, 500m, 1000m, and 1500m).

There is another interesting point shown in Fig.6b. At early stage of development, the spatial scale of the echos was rather small, i.e., less than 10 km in the direction perpendicular to the storm system. After the storm reached its mature stage in Taipei basin (at around 1505 LST), the echos extended to its maximum horizontal scale. At this time, the major convective precipitation radar echos were concentrated in the basin area. To the east of convective echos, the stratiform precipitation radar echos were present but in a much weaker state than what usually observed in a mature midlatitude or tropical squall line system (Houze, et al., 1989).

5. Vertical structure of the storm

a. Precipitation structure

Fig.7 showed a sequence of vertical cross sections of reflectivity (thin solid lines). The cross section was chosen to pass through Taipei basin to show the vertical structure evolution of storm B. At early stage (1305 LST, Fig.8a), the convection was shallow with echo top (defined by 10 dBZ contour) reached only 5 km height. It is noted the first echo was found over the mountain top area at 1035 LST with similar vertical echo structure (figure not shown). After initiation, the storm propagated slowly westward down the mountain slope without significant development. At 1405 LST (Fig.7b), the storm propagated to the edge of the basin, and rapid development started. The echo top penetrated above 12 km height. The maximum reflectivity of the storm was larger than 45 dBZ and occupied a large area. At this stage, the

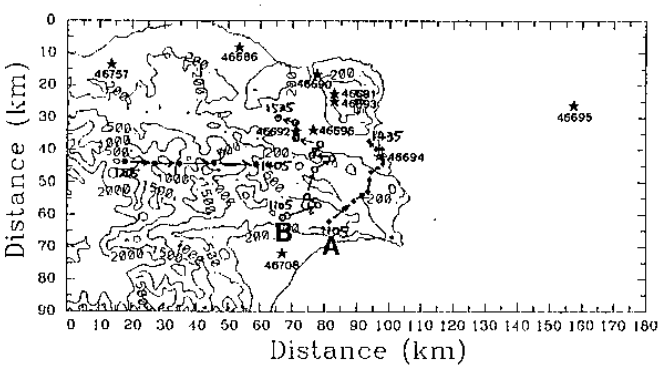

Fig.5. Trajectories of the three major convective precipitation centers on 21 June 1991 derived from the sequential radar reflectivity maps in time interval of 30 minutes.

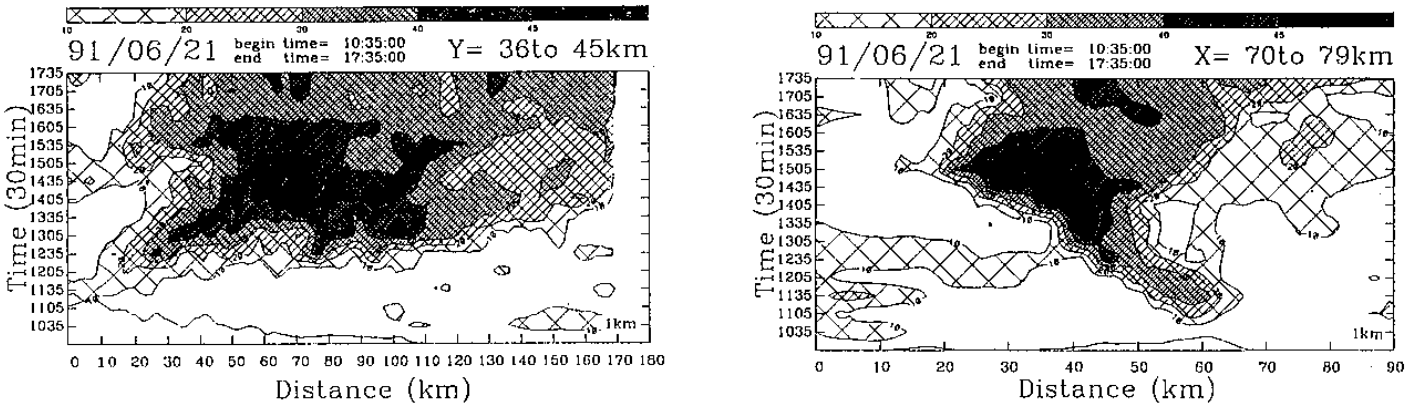

Fig.6. Time evolution of maximum radar reflectivity in a vertical column in (a) northeast-southwest (36-45 km) and (b) northwest-southeast (70-79 km) cross sections passing Taipei basin. The beginning contour is 10 dBZ and increase by 10 dBZ. The terrain feature is shown at the bottom of the figure.

storm showed an intense upright feature without significant stratiform precipitation signature. At 1505 LST (Fig.7c), the storm reached its mature stage. The major convective precipitation region was largely in Taipei basin. The 30 dBZ reflectivity contour reached 12 km height suggesting the existence of a very strong convective upward motion. At this time, the storm started to develop its stratiform precipitation region to the east of major convective precipitation area. The reflectivity pattern showed a slightly eastward tilt at this stage.

b. Flow structure

Fig.7 also showed a sequence of vertical cross sections of winds perpendicular to the storm system derived from CAA Doppler radar's radial velocity data. Since the radial velocity only sampled partial component of the true total velocity, the derived wind field could only be interpreted in a qualitative manner. The light-shading is flow from right (easterly component) with magnitude less than 5 m/s, the heavy-shading and heavier-shading is flow from left (westerly component) with magnitude less than 5 m/s and larger than 5 m/s, respectively. The structure in Fig.7a revealed several different flow regimes during this relatively undisturbed period. Weak westerly winds prevailed in most of the troposphere at earlier stage. On top of mountain, weak easterly winds (< 5 m/s) were present in the lower troposphere. On western slope and Taipei basin area, on the other hand, a stronger westerly winds (> 5 m/s) were present in the lowest 1 km. The strong westerly winds in the atmospheric planetary boundary layer on the western slope of Central Mountain Range on middle of the day suggested the thermally driven sea-breeze front could not only penetrate inland toward the base of the mountains, but also be lifted over the sloping region. Similar result was documented in Johnson and Bresch (1991) and Chen et al. (1991).

In Fig.7b, the structure was abruptly changed. The sea-breeze front was lifted to higher altitudes revealed a structure of vertical transport of horizontal momentum due to an intense convective activity. Accompanying with the strong convective activity, winds in atmospheric PBL over the sloping terrain showed an abrupt change from strong westerly to weak easterly. By referring to the reflectivity pattern, the occurrence of this abrupt change of wind direction was casued by the heavy precipitation associated with the storm. This results were consistent with the surface station observations that the heavy precipitation was accompanied by abrupt wind change. Furthermore, it is reasonable to infer from surface observations that the air in this pool of easterly was relatively colder than what was in the westerly flow due to evaporation. From above discussion, Fig.7b suggested that the existence of sea-breeze front over the sloping terrain provided a very important lifting mechanism for storm intensification, and the precipitation-induced outflows which had a larger component in the direction of downslope interacted closely with the see-breeze seemed to provide another important lifting force in maintaining the storm system.

Fig.7c showed the flow structure at the mature stage. The major feature of this diagram was the presence of the stratiform precipitation region east of the major convective precipitation region. Smull and Houze (1987) discussed the flow structure and formation mechanism of the trailing stratiform precipitation. They showed, within the stratiform cloud, there is a layer of upward-sloping, front-to-rear flow emanating from the upper portions of the convective line. This flow, which contains mesoscale ascending motion, advects ice particles detrained from the convective cells rearward. The ice particles slowly fall as they are carried rearward and eventually to form aggregates. The aggregates fall through 0°C level and melt, produce the radar bright band. Our results showed within the stratiform precipitation region, the westerly winds were slightly intensifed. The presence of mesoscale upward-sloping flow was suggested. However, the reflectivity field did not show any evidence of bright band in this case.

6. Discussion and concluding remarks

In order to gain a better understanding of storm propagation, the winds from sounding of Panchiao taken at 8 am 21 June 1991 was reconstructed into parallel (u) and perpendicular (v) components with respect to the storm propagation direction, i.e., northwest-southeast (Fig.8). It showed the u-component environmental wind (parallel to the storm movement) was rather weak in magnitude, less than 5 m/s in most levels. The directions of u were westerlies in most levels with some easterlies in lower troposphere. The v-component environmental wind was stronger (about 10 m/s) and in the direction from the south. This environmental wind structure provided some important clues to storm propagation and organization. The major enviromental winds were deep-layer monsoonal southwesterlies. Hence, the convective cells initiated on top of mountains due to thermal heating chiefly propagated in the direction of this flow. Besides this, the outflows generated by precipitation had its largest component in the direction of maximum mountain slope where new cells were most possibly to be triggered. Thus, the storm movement due to these two causes should be in north-northwest direction if the initial cell was formed east of Taipei basin and in northeast direction if the inital cell was formed south of Taipei basin. This argument is consistent with what was observed by tracing radar echos.

The storm intensity was weak during its early life stage. Above argument is valid in this situation. Nevertheless, as the storm moved to the edge of the mountain, the see-breeze front apparently played an

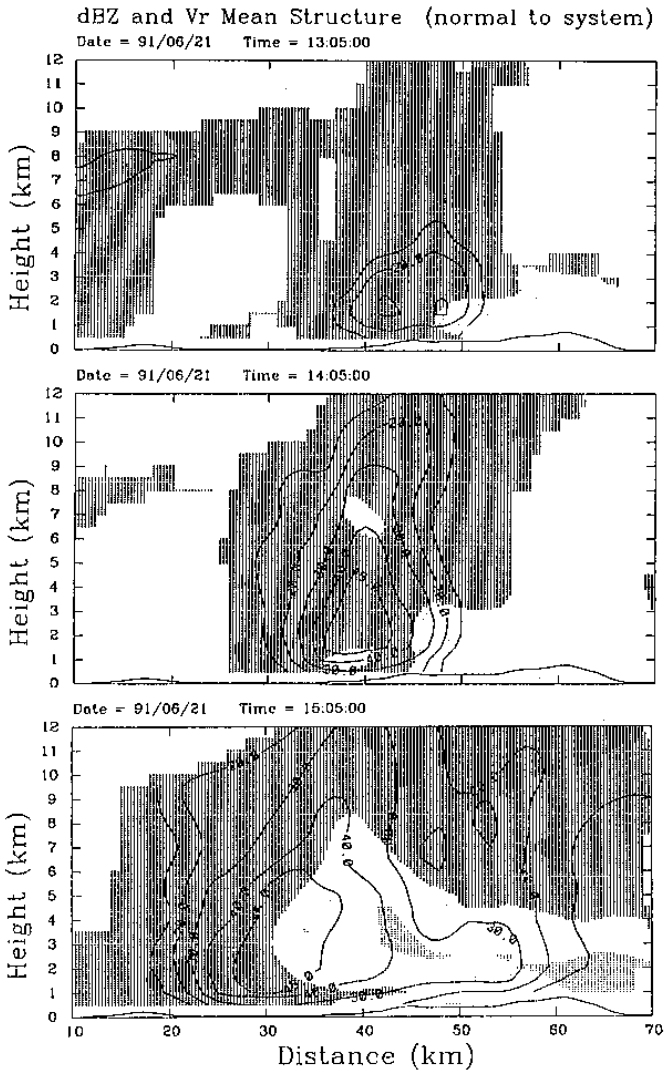

Fig.7. The radar reflectivity and the wind component perpendicular to the storm orientation derived from CAA Doppler radar at 1305 (a) and 1405 LST (b) 21 June 1991 in a northwest-southeast cross section passing Taipei basin. The contour lines are reflectivity. The light-shading represents flow from the east and the heavy-shading represents flow from the west.

important role to intensify the storm as shown in vertical cross sections. As storm intensifed, the relatively weak environmental flow was less important to storm motion. The storm revealed a quasi-stationary charater and moved slowly toward west-southwest in its mature stage. At this time, the storm was in the basin area, hence, the sloping trrrain effect is not existent. Therefore, the storm propagation could be attributed majorly to its own dynamic necessity, i.e., toward the inflow region where fresh warm and moist air located.

From above discussion, we have seen that the complex terrain features in Taiwan could play such a subtle role in controlling the organization, propagation, and development of the mesoscale precipitation systems over the Island. This paper only delivers a little flavor. Further studies on this issue are definitely necessary and fruitful.

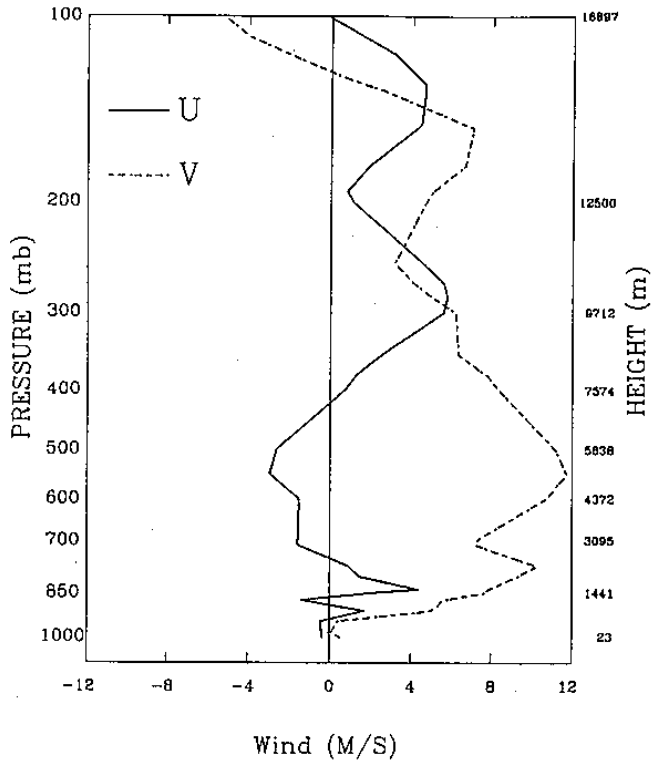

Fig.8. The normal and the parallel components of wind taken from the sounding of Panchiao on 0000 UTC 21 June 1991.

Acknowledgements

Support of this research was partially provided by the National Science Council of Republic of China under grant NSC81-0414-P002-03B and NSC82-0202-M-002-159.

References

Chen, C.-S., W.-S. Chen, and Z.-S. Deng, 1991: A study of a mountain-generated precipitation system in northern Taiwan during TAMEX IOP8. Mon. Wea. Rev., 119, 2574-2606.

Cotton, W. R., and R. A. Anthes, 1989: Storm and Cloud Dynamics. Academic Press, San Diego, 883 pages.

Houze, R. A. Jr., S. A. Rutledge, M. I. Biggerstaff, and B. F. Smull, 1989: Interpretation of DOppler weather radar displays of midlatitude mesoscale convective systems. Bull. Ame. Meteor. Soc., 70, 608-619.

Johnson, R. H., and J. F. Bresch, 1991: Diagnosed characteristics of precipitation systems over Taiwan during the May-June 1987 TAMEX. Mon. Wea. Rev., 119, 2540-2557.

Smull, B. F., and R. A. Houze, 1987: Dual-Doppler radar analysis of a midlatitude squall line with trailing region of stratiform rain. J Atmos. Sci., 44, 2128-2148.

Tao, W.-K., and J. Simpson, 1984: Cloud interactions and merging: numerical simulations. J. Atmos. Sci., 41, 2901-2917.

北台灣地區地形引發之中尺度降水系統
－單都卜勒雷達資料之應用

周仲島　秦玉璽
台灣大學大氣科學研究所

摘　要

本研究利用中正機場都卜勒雷達資料探討一地形引發之中尺度對流系統的發展、移行、與組織。此中尺度對流系統在台灣北部地區，尤其是台北盆地及基隆地區，於短短三小時內帶來超過120毫米的雨量（10分鐘雨量有達到 40毫米的紀錄），造成頗爲嚴重的積水現象。本論文特別針對環境風切場、海風鋒面、地形斜坡，以及伴隨對流系統之外流邊界等控制對流演化的物理因子間交互作用過程，予以剖析。

1992年6月21日早上地面鋒面正逐漸接近本省北部，台灣地區盛行微弱但深厚的西南氣流。當時大氣相當溫暖而潮濕，具有甚大的對流可用位能。台北測站地面溫度在早上8時爲26.4℃，而在11時42分已上升至33.1℃，顯示日照相當充份。由上述環境條件可預期海岸地區將有顯著海風，且山區快速加熱，有利熱力引發之雷雨系統發展。

散亂無組織之雷雨胞在中央山脈北端之山區，於11時開始發展，迅即在1小時內連成一條東北－西南走向的雷雨帶。此雷雨帶沿北部山區西側斜坡緩慢下移（平均移速小於3m／s），其強度持續增強，於下午2時進入台北盆地。在盆地內幾呈滯留，並維持其強度。至下午4 時後始逐漸減弱、消退。經過仔細追蹤每半小時雷達回波資料，發現主要雷雨系統的移行分爲兩部份，在台北盆地南側較高山區形成之雷雨系統係往東北偏北方向發展。而在台北盆地東側山區形成之雷雨系統係沿西北偏西方向發展。經分析結果發現兩類雷雨系統的發展，皆是沿最大地形斜坡與中低對流層盛行風合成向量的方向。

利用都卜勒雷達徑向風場及地面測站資料分析結果發現，因海陸加熱差異形成的海風鋒面，在中午時分由西海岸已可深達內陸30公里至西側斜坡底處，且有在斜坡處被抬舉的現象。當地形引發之雷雨系統沿地形斜坡下滑時，在西側斜坡底處與海風鋒面相遇，此時雷雨系統得以迅速增強，並組織成中尺度強對流降水系統，發展高度可達12公里以上。此降水系統經過台北盆地時，地面測站資料顯示，大量對流性降水伴隨此雷雨系統，地面氣壓迅速上升（1.5 毫巴），氣溫、露點急劇下降（7℃），風向由西風變成東風，顯示伴隨中尺度降水系統的外流邊界現象頗爲顯著。新生雷雨胞在外流邊界與海風交界處持續得以發展，並達到成熟，此時整個系統的移動速度相當緩慢，幾呈滯留，因此降水相當集中。

自1987年TAMEX實驗以來，我們對於造成台灣地區局部地方豪雨的災害天氣現象，經由大家的共同努力，不論在梅雨鋒面的結構與動力，中尺度對流系統的結構與動力，以及台灣地形對天氣現象的影響等，已有初步的認識。然而形成中尺度災害天氣的過程是如此複雜，同樣的控制因子若是運作的程序或方式稍有差異，形成的結果可能南轅北轍。這方面的認知在過去的研究中仍相當缺乏。本文所提供的例子顯示在日照條件充沛的情形下，台灣的地形及海陸分佈，在微弱綜觀環境條件，如何與山區形成之熱雷雨系統，經由降水過程產生的外流邊界相互運作決定雷雨系統的發展，組織與移行。類似的現象非常值得利用數值模擬方法進一步的探索，以確切了解台灣地區複雜地形在激發與組織對流系統所扮演的角色。另一方面，單都卜勒雷達資料在天氣預報與分析作業上的應用，亦顯得相當不足。尤其是都卜勒雷達在觀測徑向風場方面的特有功能，幾乎可以說是少有發揮。在此研究中，我們特別說明如何利用分析技巧，充份掌握海風鋒面的結構與移行，使我們對於此個案中雷雨系統在進入盆地時得以被快速加強的現象，提供較合理的解釋。